6-2020

Effect of hydrothermal temperature treatment on the variance of fluorescence in Ca2SiO4:Tb3þ

Rajaboopathi Mani

Santosh K. Gupta
The University of Texas Rio Grande Valley

Recommended Citation

Mani, R., & Gupta, S. K. (2020). Effect of hydrothermal temperature treatment on the variance of fluorescence in Ca2SiO4:Tb3+. Journal of Science: Advanced Materials and Devices, 5(2), 250–255. https://doi.org/10.1016/j.jsamd.2020.03.001

Journal of Science: Advanced Materials and Devices 5 (2020) 250–255

Contents lists available at ScienceDirect

Journal of Science: Advanced Materials and Devices

journal homepage: www.elsevier.com/locate/jsamd

Original Article

Effect of hydrothermal temperature treatment on the variance of fluorescence in $Ca_2SiO_4:Tb^{3+}$

Rajaboopathi Mani [a], [*], Santosh Kumar Gupta [b], [c]

[a] Centre for Research and Development, Department of Physics, PRIST Deemed to be University, Vallam, Thanjavur, 613403, Tamil Nadu, India
[b] Radiochemistry Division, Bhabha Atomic Research Centre, Trombay, Mumbai, 400085, India
[c] Department of Chemistry, University of Texas Rio Grande Valley, 1201 West University Drive, Edinburg, TX, 78539, USA

ARTICLE INFO

Article history:
Received 29 November 2019
Received in revised form
26 February 2020
Accepted 4 March 2020
Available online 13 March 2020

Keywords:
Hydrothermal method
Dicalcium silicate
Photoluminescence
Valence band
Inorganic phosphors

ABSTRACT

Investigations of structural defects and their associated impact on the optical properties of optical materials are essential expediencies because different methods are involved in the preparation of those materials for display applications. Lanthanide ion doping is a simple structural probing strategy that facilitates the challenges of identifying the structural defects. Pure and terbium (Tb^{3+}) doped Ca_2SiO_4 (C_2S) particles were prepared using Pechini (C_2SP) and hydrothermal methods (C_2SH). From SEM images, it is observed that the Tb^{3+} doped C_2SP particles were highly agglomerated, more than the C_2SH particles. The TEM study confirmed that the particle size decreased for C_2SH prepared at the high hydrothermal temperatures of 180 and 200 °C (C_2S:180H and C_2S:200H). Fluorescence emission quenching occurred for Tb^{3+} doped C_2S:180H and C_2S:200H. The emission intensity was high for Tb^{3+} doped C_2SH prepared at 140 °C compared to Tb^{3+} doped C_2SP, C_2S:180H and C_2S:200H. The changes in the O2p orbitals, associated with the upper-level valence band spectra of the tetrahedral silicate of pure C_2SP and C_2S:180H, were experimentally evaluated in the X-ray photoelectron spectroscopy (XPS)-valence band spectra. The symmetry lowering owing to the distortion in the silicate unit quenched the emission, which was confirmed by XPS-valence band spectra and Tb^{3+} emission lines. This study suggests that the Pechini method is more suitable to prepare the Tb^{3+} doped C_2S phosphors compared to the hydrothermal method, particularly at high temperature for solid state display and scintillator applications.

1. Introduction

The β-dicalcium silicate (Ca_2SiO_4, C_2S) is a component of Portland cement responsible for later strength of the concrete [1]. The hydration rate of C_2S is low compared to tricalcium silicate (Ca_3SiO_5, C_3S) and needs to be enhanced. In addition to differences in the Ca to Si ratio in C_2S and C_3S, the distinct oxygen coordinations of Ca and Si also differentiate the structures [2]. The energy gap is 5.3 eV for C_2S and 4.1 eV for C_3S. Local atomic distortions, i.e. changes in oxygen coordination associated with Ca and Si due to different dopants, were theoretically elucidated for the improvement of the C_2S hydration rate [3,4]. The lanthanide (Ln) doping is an excellent method to probe the local structure of a host lattice, especially for the interaction distance between oxygen and the host cation [5,6]. The emission lines from the Ln ions are strongly influenced by the presence of oxygen in the lattice. For instance, the slight distortion in the SiO_4^{4-} tetrahedra in C_2S decreases the symmetry and thus changes the position of the Ca ions. The radiative transition rate is closely related to the local symmetry of the emission centres [7]. Many Ln dopants such as Eu^{2+}, Eu^{3+}, Ce^{3+}, Er^{3+}, Dy^{3+} occupy the Ca site of C_2S and the resulting slight distortion in symmetry will be reflected in the emission lines [8–11]. The X-ray photoelectron spectroscopy (XPS) valence band spectra can also experimentally demonstrate the local structure distortion as it contains information about the O2p atomic orbitals associated with the C_2S silicate unit.

The influence of preparation methods on the structure and fluorescence properties of Eu^{3+}doped fluoride powder has been reported before [12,13]. Our group recently recorded the changes in structural distortion owing to a hydrothermal treatment and an aliovalent dopant (Eu^{3+}) for C_2S [14]. The green emission at around 544 nm, due to the $^5D_4 \rightarrow {}^7F_5$ transition that is allowed by electric

---

[*] Corresponding author. Department of Chemical and Metallurgical Engineering, School of Chemical Engineering, Aalto University, P.O. Box 16100, FI-00076, Aalto, Espoo, Finland.
E-mail address: mrajaboopathi@gmail.com (R. Mani).
Peer review under responsibility of Vietnam National University, Hanoi.

https://doi.org/10.1016/j.jsamd.2020.03.001

dipole transitions (EDT) of terbium (Tb^{3+}), is highly sensitive to the local environment around the Tb^{3+} (but not so hypersensitive as Eu^{3+}) and its intensity depends on the symmetry of the crystal field. On the other hand, the blue emission at about 488 nm, due to the $^5D_4 \rightarrow {}^7F_6$ transition that is allowed by magnetic dipole transitions (MDT) of Tb^{3+}, hardly varies with the crystal field strength [15]. Their ratio gives information about structural changes in the host. Moreover, the Tb^{3+} ion is an excellent doping ion from the perspective of exploring novel green phosphors.

The valence band spectrum contains information about the density of electrons associated with the valence band maximum (VBM) (it is equivalent to the highest occupied molecular orbital (HOMO) in the molecular level scheme) located around oxygen which involves a covalent bonding with silicon atoms to form a silicate group. The valence band analysis of C_2S is essential because it has information about the O2s and O2p orbitals of silicate in C_2S similar to vitreous silicate [16]. To our knowledge, there is no report on the VB of C_2S. Therefore, this report also discusses the valence band spectra of C_2S obtained from X-ray photoelectron spectrometry (XPS). The upper valence band spectra of C_2S are associated with the Si Sp^3-O2$p_x\pi$-bonding and the Si-non bridging oxygen (NBO) of the Si Sp^3-O 2p_z σ-bonding character of O2p oxygen. The changes in this level can clearly give information about the structural distortion related to the $SiO_4{}^{4-}$ tetrahedra in C_2S.

In this work, we report on the influence of different preparation methods on the fluorescence properties of Tb^{3+} doped C_2S. The structural distortion and associated impact on the symmetry lowering of C_2S have been probed by Tb^{3+} emission spectra. The valence band spectra of C_2S experimentally reveal the distortion associated with the silicate unit. Since the hydrothermally prepared samples show emission quenching for Eu^{3+} doped C_2S in ref. [14], the Tb^{3+} doped C_2S was prepared using a hydrothermal method and its impact on the emission properties was explored. The Pechini method produces pure particles in which high temperature and pressure have not been involved during the synthesis. Therefore this can be taken as a reference to compare the hydrothermally prepared samples to identify the effect of high temperature and related pressure. The morphology of Tb^{3+} doped C_2SP and C_2SH has been recorded by scanning electron microscopy (SEM). The changes in the valence level of C_2SP and C_2S:180H have been experimentally revealed by the XPS valence band spectra. The fluorescence emission and decay curves helped us to elucidate the structural distortion due to the hydrothermal treatment.

2. Experimental

The pure and Tb^{3+} doped C_2S samples were prepared by Pechini and hydrothermal methods. All the chemicals were analar grade and used as received. In the Pechini method, the calculated amounts of calcium nitrate and colloidal silica with a molar ratio of two were dissolved in water separately and then citric acid (CA), with a molar ratio of CA to total cation equal to one, was added. The ethylene glycol (EG) was further added with a molar ratio of EG to CA equal to two. The final solution was stirred for an hour and then heated at 70 °C under fume hood in order to evaporate the excess liquid. The product was dried at 140 °C for 12 h and then calcined at 800 °C for 3 h to obtain the C_2SP (P denotes the Pechini method).

In the hydrothermal method, after preparing the solution as discussed above, it was moved to a 40 mL Teflon lined autoclave for the hydrothermal treatment at different temperatures of 140 °C, 180 °C and 200 °C for 20 h at an autogenous pressure. The final solution was clear after hydrothermal treatment at 140 °C. For the 180 °C and 200 °C samples, the treated solution was a colloid -like gel and was centrifuged and then washed with water followed by ethanol. All the products were dried separately at 140 °C for 12 h in the oven and then calcined at 800 °C for 3 h to obtain C_2S:140H, C_2S:180H and C_2S:200H (H denotes hydrothermal method). Tb $(NO_3)_3 \cdot 6H_2O$ was used as a source for Tb^{3+} to prepare Tb^{3+} doped C_2S in both methods.

3. Characterization techniques

As we already reported the basic structural findings for the C_2S samples in our earlier report [14], here we used SEM, XPS-valence band spectrum and photoluminescence spectra for further investigations. The powder XRD patterns of the 4% Tb^{3+} doped C_2SP and C_2S:180H were recorded using the Bruker AXS-D8 Advance diffractometer with Cu Kα radiation ($\lambda = 1.5406$ Å) at 40 kV over the 2θ range of 10–70°. Compared to the pure XRD pattern of C_2S, there is no significant difference in the C_2SP:4%Tb^{3+} and C_2S180H:4%Tb^{3+} patterns except for the reduced intensity in the latter case (Figure S1, see supplementary information). It can be presumed that, since the Tb^{3+} dopant occupies the site of Ca^{2+}, there is no significant change in the phase or crystal structure of C_2S due to the dopant. It further confirms that the dopants occupy the Ca^{2+} site. The morphologies of the pure and Tb^{3+} doped samples were examined using a Hitachi-S-4800, Japan scanning electron microscope. The particle sizes and SAED patterns were recorded using JEOL JEM-2100 TEM microscopy. The samples were placed on a metal stud using a carbon tape and then dried under vacuum to cover approximately 10 nm of gold coating. The XPS spectra were recorded on a Thermo Scientific ESCALAB 250, Germany, equipped with Al Kα radiation at 1486.6 eV. The spectral peaks were fitted with the CasaXPS software using Gaussian–Lorentzian (30% Lorentzian) line shapes. The background was subtracted using the Shirley method. The charging effect and corresponding binding energy shift for all the elements have been calibrated for the charging adventitious carbon 1s peak at 284.6 eV. A high-resolution spectrofluorometer (UK, Edinburg instrument FLS920) was used to record the solid-state photoluminescence spectra and decay curves. The Xenon lamp was used as an excitation source for the emission and excitation spectra, and the laser for the decay curve measurement.

4. Results and discussion

4.1. SEM and TEM microscopy

Scanning electron microscopy records the morphology of C_2SP, C_2SP:Tb^{3+} and C_2S180H:Tb^{3+} and the images are shown in Fig. 1. The C_2SP showed chunky solids (see supplementary Figure S2) comprising a spherical plate-like morphology or a tiles-like interlocking as shown in the Fig. 1a. From the TEM images, one can find that the high hydrothermal temperature of 180 °C reduces the mean particle size as shown in the Figure S3 (c, d). The particle size is $\geq$ 100 nm for C_2SP and around $\leq$50 nm for C_2S:180H. The C_2SP particles are more agglomerated than those of C_2S:180H and the sizes of these particles are not of an uniform shape. The ring pattern (polycrystals) for C_2S:180H and the nearly spot pattern for C_2SP of the selected area for the electron diffraction (SAED, Figure S3 a,b) pattern clearly indicate the reduced particle size. A similar particle size reduction has been reported elsewhere [17]. The observed planes (236), (130), (200) belong to C_2S and match well with PDF 360–642. For the C_2SP:Tb^{3+} (Fig. 1b) the particle morphology remains the same and there is no pronounced change in it. Though the aliovalent dopant can change the electron density of the dopant or its surrounding and thus controls the particle growth [17,18], the reduced particle size is owing solely to the hydrothermal treatment since the dopant concentration is low.

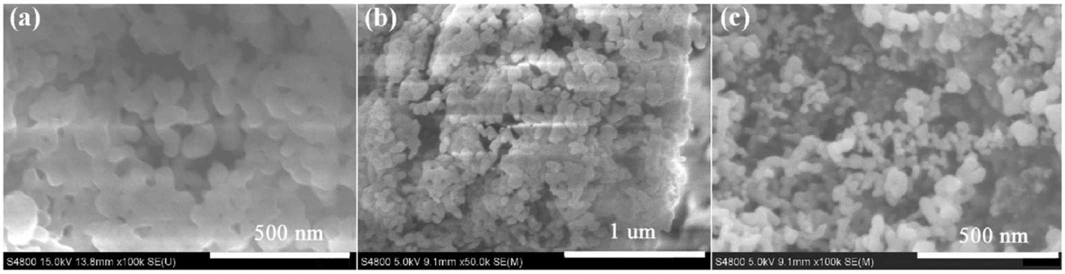

Fig. 1. SEM images of C_2SP (a), $C_2SP:Tb^{3+}$ (b) and $C_2S180H:Tb^{3+}$ (c).

4.2. *XPS valence band spectra of C_2S*

The effect of a hydrothermal treatment on the silicate tetrahedra in pure C_2SP and C_2S:180H can be analysed by the XPS valence band spectra. The C_2S spectra have three sub-bands namely, O2s and a lower and upper valence band (LVB and UVB); the latter two bands are associated with O2p (Fig. 2). The bridging oxygen (BO; O—Si—O) and non-bridging oxygen (NBO; O—Si-M_{etal}) bonds are observed at 27.52eV and 24.93eV for C_2SP and at 27.50 eV and 24.99 eV for C_2S:180H, respectively. The absence of a change in the binding energy (BE) position of the peaks indicates that the electron density remains the same. The fwhm of the NBO has narrowed whereas BO has little broadening for C_2S:180H compared to C_2SP. It indicates changes in the surrounding of the Si-bridging and non-bridging interactions. There is no shoulder peak at the high BE side of O2s, which has been observed for Sr_2SiO_4 elsewhere [17]. The LVB and UVB are associated with the overlap of O2p atomic orbitals and Si-sp3 hybridized atomic orbitals. For instance, the LVB consists of Si-BO σ-bonding of Si Sp^3-O $2p_z$ character. The Si Sp^3-O$2p_x$π-bonding and Si-NBO of Si Sp^3-O $2p_z$ σ-bonding are associated with UVB. The changes in the binding energy associated with LVB and UVB attracted the research focus as they reflect the electron density changes in the highest occupied molecular orbitals levels. In C_2SP, the area of the peak associated to UVB is high whereas it is low for LVB. It is flipped for C_2S:180H. Particularly, the LVB has gained intensity and its broadness of the peak indicates the dispersed band associated with it. The BE of UVB has been red shifted. The orbital character of C_2SP has somehow been disturbed compared to C_2SH which is clearly observed in the fwhm, i.e., changes in intensity and BE of LVB and UVB. Particularly, since the UVB band is unstable (more energetic) than the LVB band, that may have been affected by the hydrothermal temperature. The area of UVB decreased, at the same time it increased in LVB from C_2SP to C_2S:180H. It further confirms our previous results that the distortion in the SiO_4 polyhedra is due to hydrothermal treatment [14]. The impact of particle size reduction from C_2SP and C_2S:180H on the valence band spectra is not straightforward in our case because the particle sizes of both are within the nanometer range. This distortion can change the Ca—O distance. When Tb^{3+} replaces Ca, this change can be reflected in the emission spectrum as discussed in the following Section 4.3.

4.3. *Fluorescence spectroscopy: pure and Tb^{3+} doped C_2SP and C_2SH*

Fluorescence excitation and emission spectra of 3–5% of Tb^{3+} doped C_2S:140H are presented in Fig. 3a, and 3b. The excitation band, observed around 242 nm, is monitored at the emission wavelength of 540 nm. The emission quenching at 5% of Tb^{3+} in C_2S:140H has been observed. The critical transfer distance (Rc) between the dopant ions responsible for the quenching can be calculated using the Blasse equation [19].

$$R_C = 2\left(\frac{3V}{4\pi N X_C}\right)^{\frac{1}{3}} \tag{1}$$

where V is the volume of the unit cell, X_C the critical concentration at which the quenching occurs and N the number of available crystallographic cationic sites to occupy the activator ions. In C_2S, the unit cell volume is $V = 1036.31$ Å^3 containing $Z = 4$ formula units. There are two calcium ions in one formula unit so that $N = 8$ calcium sites can be occupied by Tb^{3+} ions. Considering $X_C = 5.0\%$ (0.050), the R_c in Tb^{3+} doped C_2S:140H was calculated to be 17.042 Å. In this case, the Tb^{3+}- Tb^{3+} distance is much higher than 10 Å so that the electric multipolar interaction is responsible for the non-radiative energy transfer among the Tb^{3+}ions in C_2S:140H Tb^{3+}. The concentration quenching by a reabsorption mechanism is ruled out (see Table 1).

The excitation and emission spectra of samples prepared with 4% of Tb^{3+} doped in C_2SP, C_2S:140H and C_2S:180H are presented in

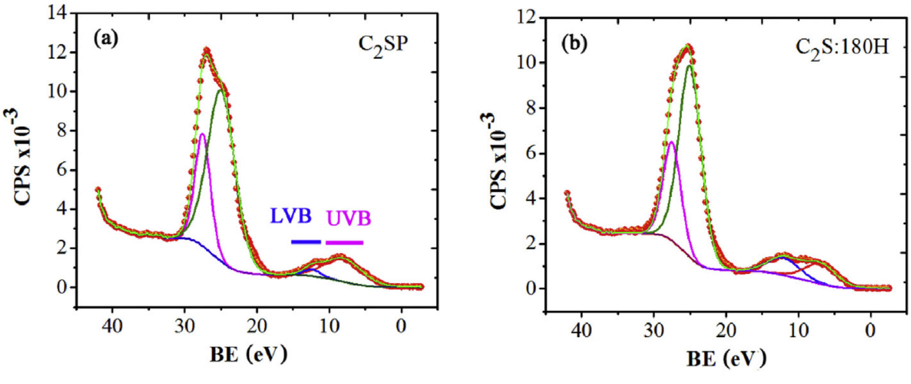

Fig. 2. Valence band spectra of pristine C_2SP (a) and C_2S:180H (b). The LVB and UVB represent the lower and upper valence bands.

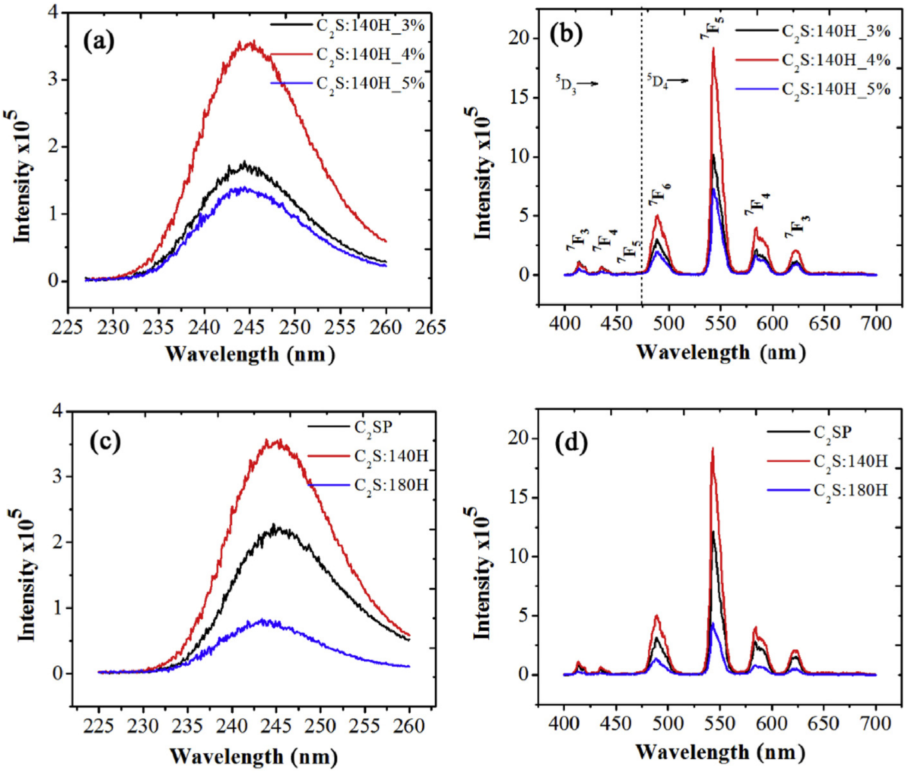

Fig. 3. The excitation (a, c) and corresponding emission spectra (b, d) of Tb^{3+} doped C_2SP and C_2SH. The concentration of Tb^{3+} is varied with 3–5% to optimise the absorption and emission intensity of C_2S:140H (a, b). The 4% of Tb^{3+} doped C_2S:140H shows strong absorption and emission so that this concentration was used to dope Tb^{3+} into C_2SP and C_2S:140H and C_2S:180H samples (c, d).

Table 1
Fitted values of valence band spectra of C_2SP and C_2S:180H.

C_2SP	BO	NBO	LVB	UVB
Position	27.5206	24.9390	12.3397	8.0092
fwhm	2.50266	4.50774	2.78836	6.06205
Area	15584.1	42692.4	1005.9	7833.6
C_2S:180H				
Position	27.5084	24.9996	12.0500	6.9133
fwhm	2.8828	3.67104	5.19054	5.16059
Area	13608.2	33690.7	4339.8	4939.6

Fig. 3c and 3d. The emission lines are due to the transition of $^5D_4$ to ^7F_j (j = 3, 4, 5 and 6). The $^5D_4 \rightarrow {}^7F_5$ line at 544 nm (EDT) varies strongly compared to the $^5D_4 \rightarrow {}^7F_6$ line at 488 nm (MDT) (Fig. 3b and 3d). It can be predicted that Tb^{3+}ions have occupied two different sites but the majority of the Tb^{3+} ions occupy relatively symmetric environments in C_2S. The EDT arises due to the localization of Tb^{3+} at the CaO_8 site whereas a small fraction of Tb^{3+} at the CaO_7 site leads to MDT at 488 nm. The asymmetric ratio value (R) has been calculated by $R = I(^5D_4 \rightarrow {}^7F_5)/I(^5D_4 \rightarrow {}^7F_6)$ and its values are 3.8070, 3.9207 and 3.2388 for Tb^{3+} doping of C_2SP, C_2S:140H and C_2S:180H, respectively. The low R-value of $C_2S180H:Tb^{3+}$ indicates that the Tb^{3+} ions occupy sites of lower symmetry than in the other two samples. The symmetry lowering probed by the Tb^{3+} dopant may be due to changes in the environment around the host cation, in other words, the distortion in the silicate unit changes the Ca–O distance.

The hydrothermal treatment enhances the emission of Tb^{3+} doped C_2S:140H compared to Tb^{3+} doped C_2SP. For C_2S:180H, the increased hydrothermal temperature quenches the emission. To further confirm the quenching, the hydrothermal temperature was increased to 200 °C and the emission spectra were recorded as presented in Figure S4 (see supplementary). As expected, the emission has further been quenched. The observed high and low emission intensities of the hydrothermally prepared sample must be related to a distortion in the silicate unit of the host lattice and to some surface defect and/or impurity. The distortion in the silicate unit due to the hydrothermal treatment has already been revealed by the XPS valence band spectra in Section 4.2.

It is also important to consider the possible occurrence of carbon impurities such as C–O, C–H and C–C because the C_2S sample has been prepared with the use of citric acid and ethylene glycol [20]. However, since all the samples were calcined at 800 °C, the role of impurities on the fluorescence spectra can be considered to be minimal because most of the carbon-related impurities are removed at the high calcination temperatures [20]. If an impurity is formed at any localized occupied state, this emission quenching should have been observed in all the samples and not only for the hydrothermally treated samples. It is further clear by the FTIR results that there are no pronounced changes in the spectra of those impurity regions but changes at silicate region as presented in ref. [9]. Other studies may be required to confirm the presence of the carbon impurities.

The emission quenching, particularly observed for C_2S:180H and C_2S:200H, ensured the effect of the hydrothermal treatment of the samples at high temperature. As reported earlier for C_2S, Eu^{3+} doped C_2SH shows about 10 nm of a blue shift of the charge transfer band (CTB) compared to C_2SP. It reminds to the extended distance of O^{2-}–Eu^{3+} which was attributed to changes in the oxygen network associated with the silicate unit that, consequently, alter the CTB distance [14]. This distortion suppresses the fluorescence emission intensity of $C_2S180H:Tb^{3+}$ and $C_2S200H:Tb^{3+}$ samples prepared at high hydrothermal temperatures.

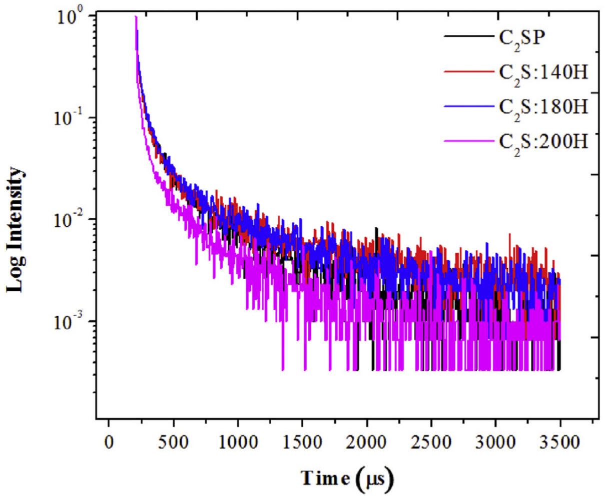

Fig. 4. Decay plot of Tb^{3+} doped C_2SP and C_2SH.

Table 2
Lifetime values of Tb^{3+} doped C_2SP and C_2SH.

Lifetime/Tb^{3+}	C_2SP	C_2S:140H	C_2S:180H	C_2S:200H
T1	122.66656	10.43209	13.99253	7.03828
T2	12.33854	111.64156	137.43964	103.12024
T_{avg}	12.33865	10.4321	13.99318	7.03828

The emission quenching of $C_2SP:Tb^{3+}$ that exceeds that of $C_2S140H:Tb^{3+}$ may be due to the particle size and the agglomeration of particles/surface defects (see supplementary Figure S1). Surface defects are known to quench the emission by providing additional pathways for a non-radiative decay. There may be a decrease in surface defects in case the sample is prepared at low hydrothermal temperatures. The agglomerates in C_2SP will scatter the excitation/emission light and, therefore, the fluorescence intensity has decreased.

The decay curve of the Pechini and hydrothermally prepared Tb^{3+} doped C_2S particles is presented in Fig. 4 and the lifetime values are presented in Table 2. It has two lifetime values indicating the fact that the europium stabilizes in CaO_8 as well in CaO_7 sites. The longer lifetime value is attributed to Tb^{3+} occupying the more symmetric CaO_8 site, whereas the short-lived terbium ion is attributed to the relatively asymmetric CaO_7 site. The average lifetime value is grossly low (Table 2) for C_2SH compared to C_2SP, which points to more defects in the hydrothermally treated samples.

5. Conclusion

The pure and Tb^{3+} doped C_2S particles were prepared by the Pechini (C_2SP) and hydrothermal (C_2SH) methods. In the valence band spectra, the broadened UVB peak of C_2SP was narrowed for C_2S:180H. This has influenced the LVB and thus altered the fwhm and binding energy of C_2S:180H. The binding energy of UVB has red shifted for C_2S:180H. The variation in the O2p orbital level of C_2S:180H indicates that there is a distortion in the silicate unit due to the high hydrothermal temperature and pressure. The critical transfer distance at doping of 5% of Tb^{3+} was calculated to be 17.042 Å, which indicates that the electric multipolar interaction is responsible for the non-radiative energy transfer among the Tb^{3+} ions in C_2S:140H. The decreasing asymmetric R value of C_2S:180H (3.24) compared to C_2SP, C_2S:140H (~3.92) confirms the occupancy of Tb^{3+} at lower symmetry sites. The hydrothermal treatment enhanced the emission for $C_2S140H:Tb^{3+}$ compared to $C_2SP:Tb^{3+}$ whereas a further raise of temperature to 180 and 200 °C quenches the emission. Since all samples were calcined at 800 °C, the quenching due to carbon impurities can be considered as minimal. Furthermore, the emission quenching has only occurred at high temperature which establishes the distortion in the oxygen network and thus the alteration of the O^{2-}–Tb^{3+}distance in C_2S.

Declaration of Competing Interests

The authors declare that they have no known competing financial interests or personal relationships that could have appeared to influence the work reported in this paper.

Acknowledgements

The author R.M is grateful to the Shandong University, China, for the XPS study.

Appendix A. Supplementary data

Supplementary data to this article can be found online at https://doi.org/10.1016/j.jsamd.2020.03.001.

References

[1] K.L. Scrivener, P. Juilland, P.J.M. Monteiro, Advances in understanding hydration of Portland cement, Cem. Concr. Res. 78 (2015) 38–56, https://doi.org/10.1016/j.cemconres.2015.05.025.

[2] E. Durgun, H. Manzano, R.J.M. Pellenq, J.C. Grossman, Understanding and controlling the reactivity of the calcium silicate phases from first principles, Chem. Mater. 24 (2012) 1262–1267, https://doi.org/10.1021/cm203127m.

[3] P. Guo, B. Wang, M. Bauchy, G. Sant, Misfit stresses caused by atomic size mismatch: the origin of doping-induced destabilization of dicalcium silicate, Cryst. Growth Des. 16 (2016) 3124–3132, https://doi.org/10.1021/acs.cgd.5b01740.

[4] H. Manzano, E. Durgun, M.J. Abdolhosseine Qomi, F.J. Ulm, R.J.M. Pellenq, J.C. Grossman, Impact of chemical impurities on the crystalline cement clinker phases determined by atomistic simulations, Cryst. Growth Des. 11 (2011) 2964–2972, https://doi.org/10.1021/cg200212c.

[5] D. Van Der Voort, G.J. Dirksen, G. Blasse, Luminescence study of Eu^{3+}–O^{2-} associates in fluorides: CaF_2, $RbCdF_3$ and $RbCaF_3$, J. Phys. Chem. Solid. 53 (1992) 219–225, https://doi.org/10.1016/0022-3697(92)90048-I.

[6] Y. Hui, Y. Zhao, S. Zhao, L. Gu, X. Fan, L. Zhu, B. Zou, Y. Wang, X. Cao, Fluorescence of Eu^{3+} as a probe of phase transformation of zirconia, J. Alloys Compd. 573 (2013) 177–181, https://doi.org/10.1016/j.jallcom.2013.03.248.

[7] H. Bian, Y. Liu, D. Yan, H. Zhu, C. Liu, C. Xu, Y. Liu, H. Zhang, X. Wang, J. Mater. Chem. C. 1 (2013) 7896–7903, https://doi.org/10.1039/C3TC31446D.

[8] Y. Sato, H. Kato, M. Kobayashi, T. Masaki, D.H. Yoon, M. Kakihana, Tailoring of deep-red luminescence in Ca_2SiO_4:Eu $^{2+}$ Angew, Chem., Int. Ed. 53 (2014) 7756–7759, https://doi.org/10.1002/anie.201402520.

[9] U.B. Gokhe, K.A. Koparkar, S.K. Omanwar, Synthesis and fluorescence properties of $Ca_2SiO_4:Dy^{3+}$ phosphor for solid state lighting application, J. Mater. Sci. Mater. Electron. 27 (2016) 9286–9290, https://doi.org/10.1007/s10854-016-4967-6.

[10] W. Ji, S. Ye, M.-H. Lee, L. Hao, X. Xu, S. Agathopoulos, D. Zheng, C. Fang, Y. Huang, Influence of N-anion-doping on the production and the photoluminescence properties of γ-$Ca_2SiO_4:Ce^{3+}$ phosphors and the $\beta \rightarrow \gamma$ phase transformation, J. Mater. Chem. C. 4 (2016) 3313–3320, https://doi.org/10.1039/C6TC00056H.

[11] N.T.K. Lien, N.V. Thang, N.D. Hung, N.D. Cuong, N.D.T. Kien, C.X. Thang, P.H. Vuong, D.X. Viet, N.T. Khoi, P.T. Huy, Influence of annealing temperature and Gd and Eu concentrations on structure and luminescence properties of (Y,Gd) $BO_3:Eu^{3+}$ phosphors prepared by sol–gel method, J. Electron. Mater. 46 (2017) 3427–3432, https://doi.org/10.1007/s11664-017-5322-2.

[12] M. Karbowiak, A. Mech, A. Bednarkiewicz, W. Stręk, L. Kępiński, Comparison of different $NaGdF_4:Eu^{3+}$ synthesis routes and their influence on its structural and luminescent properties, J. Phys. Chem. Solid. 66 (2005) 1008–1019, https://doi.org/10.1016/j.jpcs.2005.01.002.

[13] Ishwar Prasad Sahu, D.P. Bisen, Raunak KumarTamrakar, K.V.R. Murthy, M. Mohapatra, Studies on the luminescence properties of CaZrO3:Eu3+ phosphors prepared by the solid state reaction method, J. Sci.: Advanced Materials and Devices 2 (2017) 69–78, https://doi.org/10.1016/j.jsamd.2017.01.002.

[14] R. Mani, H. Jiang, S.K. Gupta, Z. Li, X. Duan, Role of synthesis method on luminescence properties of europium(II, III) ions in β-Ca2SiO4: probing local site and structure, Inorg. Chem. 57 (2018) 935–950, https://doi.org/10.1021/acs.inorgchem.7b01878.

[15] L.P. Singh, N.P. Singh, S.K. Srivastava, Terbium doped SnO_2 nanoparticles as white emitters and SnO_2:5Tb/Fe_3O_4 magnetic luminescent nanohybrids for hyperthermia application and biocompatibility with HeLa cancer cells, Dalton Trans. 44 (2015) 6457–6465, https://doi.org/10.1039/C4DT03000A.

[16] H.W. Nesbitt, G.M. Bancroft, R. Ho, XPS valence band study of Na-silicate glasses: energetics and reactivity, Surf. Interface Anal. 49 (2017) 1298–1308, https://doi.org/10.1002/sia.6262.

[17] R. Mani, S.K. Gupta, P.S. Ghosh, H. Jiang, Yellow emission from low coordination site of Sr_2SiO_4:Eu^{2+}, Ce^{3+}: influence of lanthanide dopants on the electron density and crystallinity in crystal site engineering approach, Chem. Eur J. 24 (2018) 16149–16159, https://doi.org/10.1002/chem.201803232.

[18] D. Chen, Y. Yu, F. Huang, P. Huang, A. Yang, Y. Wang, Modifying the size and shape of monodisperse bifunctional alkaline-earth fluoride nanocrystals through lanthanide doping, J. Am. Chem. Soc. 132 (2010) 9976–9983, https://doi.org/10.1021/ja1036429.

[19] G. Blasse, Energy transfer in oxidic phosphors, Phys. Lett. 28 (1968) 444–445, https://doi.org/10.1016/0375-9601(68)90486-6.

[20] C. Lin, C. Zhang, J. Lin, Phase transformation and photoluminescence properties of nanocrystalline ZrO2 powders prepared via the pechini-type Sol–Gel process, J. Phys. Chem. C 111 (2007) 3300–3307, https://doi.org/10.1021/jp066615l.